Cold atomic and molecular collisions: approaching the universal loss regime

New Journal of Physics

The open access journal at the forefront of physics

PAPER

CrossMark

Cold atomic and molecular collisions: approaching the universal loss regime

Matthew D Frye[1], Paul S Julienne[2] and Jeremy M Hutson[1]

[1] Joint Quantum Centre (JQC) Durham-Newcastle, Department of Chemistry, Durham University, South Road, Durham DH1 3LE, UK
[2] Joint Quantum Institute, University of Maryland and NIST, College Park, Maryland 20742, USA

E-mail: J.M.Hutson@durham.ac.uk

Abstract

We investigate the behaviour of single-channel theoretical models of cold and ultracold collisions that take account of inelastic and reactive processes using a single parameter to represent short-range loss. We present plots of the resulting energy-dependence of elastic and inelastic or reactive cross-sections over the full parameter space of loss parameters and short-range phase shifts. We then test the single-channel model by comparing it with the results of coupled-channel calculations of rotationally inelastic collisions between LiH molecules and Li atoms. We find that the range of cross-sections predicted by the single-channel model becomes increasingly accurate as the initial LiH rotational quantum number increases, with a corresponding increase in the number of open loss channels. The results suggest that coupled-channel calculations at very low energy (in the s-wave regime) could in some cases be used to estimate a loss parameter and then to predict the range of possible loss rates at higher energy, without the need for explicit coupled-channel calculations for higher partial waves.

1. Introduction

Elastic and inelastic or reactive collisions play a crucial role in cold atomic and molecular gases [1, 2]. Elastic collisions are used for cooling and coherent control of cold gases, whereas inelastic or reactive collisions remove atoms or molecules from traps and limit the lifetime of cold samples. Inelastic or reactive collisions have been observed in thermal samples at temperatures as low as 200 nK [3], and cold collisions can also be studied using merged [4] or decelerated [5] beams at collision energies E corresponding to tens of mK to 1 K.

In relatively simple systems, such as pairs of alkali-metal atoms or light atom-molecule systems, it is feasible to solve the many-dimensional Schrödinger equation directly using coupled-channel methods. However, for heavier and more complex systems, the number of channels required for convergence is too large and coupled-channel methods become prohibitively expensive. In this regime, considerable success has been achieved with effective single-channel methods that take account of short-range loss, whether inelastic or reactive, with a single parameter. In particular, Idziaszek and Julienne [6], Kotochigova [7] and Gao [8] have developed approaches based on quantum defect theory (QDT), which takes advantage of the fact that the short-range wavefunction is only weakly dependent on energy near threshold [9–11]. If the interaction potential $V(r)$ has an inverse power dependence on the interspecies distance r at long range, $V_{LR}(r) = -C_n/r^n$, the long-range wavefunction may be expressed in terms of the analytical solutions for the long-range potential [11, 12]. The model of Idziaszek and Julienne [6] successfully explained the temperature dependence of reactive KRb+KRb collisions at temperatures below 1 μK, and was later extended [13] to handle the additional r^{-3} dipole-dipole potential that exists when the KRb molecules are oriented with an external electric field. More recently, Jachymski *et al* [14, 15] have extended similar models up to the high-temperature limit, and used them to interpret merged-beam experiments on Penning ionization in collisions of metastable He with Ar [4].

The single-channel models can be expressed in terms of two parameters. One of these describes the probability that loss will occur when the particles reach short range, while the second describes a short-range phase shift that characterizes a background scattering length for the interaction. In the limit of complete loss at short range, the loss rate is independent of the background scattering length; this has been termed the 'universal' limit [6]. The purpose of the present paper is to undertake a systematic exploration of the behaviour of elastic and loss cross-sections as a function of these two parameters and collision energy, and also to compare the results of the single-channel model with full coupled-channel calculations on a prototype strongly coupled system, based on rotationally inelastic collisions of LiH with Li atoms.

2. Theory

The single-channel model used here assumes that loss occurs only at short range, and that flux that leaves the incoming channel does not return. To calculate the probability of reaching short range, we use a single-channel Schrödinger equation,

$$\left[\frac{-\hbar^2}{2\mu} \frac{d^2}{dr^2} + V(r) + \frac{\hbar^2 L(L+1)}{2\mu r^2} - E \right] \psi(r) = 0, \tag{1}$$

where $V(r)$ is the interaction potential, L is the partial-wave quantum number, and μ is the reduced mass of the colliding pair. We approximate the potential $V(r)$ by its long-range form $V_{LR}(r) = -C_6/r^6$; this simplification allows us to use the analytic QDT formalism of Gao [11, 16], which accurately represents the behaviour of the system across a wide range of energy around threshold [17]. Equation (1) is conveniently rescaled by the van der Waals energy and length scales $r_6 = (2\mu C_6/\hbar^2)^{1/4} = 2r_{vdw}$ and $E_6 = \hbar^2/(2\mu r_6^2)$ [11] to give

$$\left[-\frac{d^2}{dr_s^2} + U(r_s) + \frac{L(L+1)}{r_s^2} - \epsilon \right] \psi(r_s) = 0, \tag{2}$$

where $r_s = r/r_6$, $U(r_s) = V(r)/E_6$ and $\epsilon = E/E_6$. In the present case, $U(r_s) = -1/r_s^6$.

We choose to use the travelling wave reference functions of section IIIC and D of [11]. These are solutions to equation (2) that have incoming $(-)$ or outgoing $(+)$ character. They may be normalized in either the inner region i $(r_s \to 0)$ or the outer region o $(r_s \to \infty)$,

$$f^{i+}(r_s) \stackrel{r_s \to 0}{\sim} r_s^{3/2} \exp\left[-i\left(r_s^{-2}/2 - \pi/4 \right) \right], \tag{3}$$

$$f^{i-}(r_s) \stackrel{r_s \to 0}{\sim} r_s^{3/2} \exp\left[+i\left(r_s^{-2}/2 - \pi/4 \right) \right], \tag{4}$$

$$f^{o+}(r_s) \stackrel{r_s \to \infty}{\sim} k_s^{-1/2} \exp\left[+i k_s r_s \right], \tag{5}$$

$$f^{o-}(r_s) \stackrel{r_s \to \infty}{\sim} k_s^{-1/2} \exp\left[-i k_s r_s \right], \tag{6}$$

where $k_s = \epsilon^{1/2}$. Note that these differ from Gao's definitions [11] by a constant factor of $\pi^{-1/2} e^{i\pi/4}$. The reference functions in the inner and outer regions are related by

$$f^{o-} + r^{(oi)} f^{o+} = t^{(oi)} f^{i-}, \tag{7}$$

$$f^{i+} + r^{(io)} f^{i-} = t^{(io)} f^{o+}. \tag{8}$$

Equation (7) is interpreted as a wave f^{o-} travelling from the outer region inwards, which is partially reflected $(r^{(oi)} f^{o+})$ and partially transmitted $(t^{(oi)} f^{i-})$. Equation (8) is interpreted similarly for the wave f^{i+} travelling in the opposite direction. The complex coefficients t and r are functions of ϵ and L, which are readily computed from expressions given in section IV of [11] and Gao's QDT functions $Z^c(\epsilon, L)$ [18, 19]. The coefficients are related by

$$\left| r^{(io)} \right| = \left| r^{(oi)} \right|, \tag{9}$$

$$t^{(io)} = t^{(oi)}, \tag{10}$$

$$\left| r^{(io)} \right|^2 + \left| t^{(io)} \right|^2 = 1. \tag{11}$$

The short-range physics is modelled by the boundary condition

$$\psi \stackrel{r_s \to 0}{\sim} C\left(f^{i-} + S^c f^{i+} \right), \tag{12}$$

where C is an arbitrary normalization constant and S^c is the short-range S-matrix. In a true single-channel problem, S^c would be a complex number of magnitude 1, but to account for the loss of flux to other outgoing channels we allow it to have magnitude $|S^c| < 1$. We write

$$S^c = \left(\frac{1-y}{1+y}\right)e^{2i\delta^s},$$
(13)

where y is the loss parameter of Idziaszek and Julienne [6], so that $y = 1$ corresponds to complete loss at short range and $y = 0$ corresponds to no loss. The short-range phase shift δ^s may be related to the 'background'[3] scattering length a of [6],

$$\frac{a}{\bar{a}} = 1 + \cot\left(\delta^s - \frac{\pi}{8}\right),$$
(14)

where $\bar{a} = 0.477988\ldots r_6$ is the mean scattering length of Gribakin and Flambaum [20]. This allows us to map the complete range of behaviours onto the finite range $0 \leqslant \delta^s < \pi$ rather than the infinite range of $s = a/\bar{a}$ as in [6].

The formulation in terms of $|S^c| = (1-y)/(1+y)$ and δ^s makes it obvious that the collisional properties of the system are independent of δ^s (and hence of s) in the limit $y \to 1$ ($|S^c| \to 0$). We make the usual QDT approximation that S^c is independent of energy close to threshold, and also that it does not vary with partial wave L [16].

We obtain the long-range S-matrix S_L for partial wave L by matching $\psi(r_s)$, equation (12), to the usual scattering boundary conditions,

$$\psi \overset{r_s \to \infty}{\sim} f^{o-} - (-1)^L S_L f^{o+}.$$
(15)

Again, S_L would be unitary in a true single-channel problem but here it can be sub-unitary. The relationship between S^c and S_L is given by section VIIB of [11] as

$$S_L = (-1)^{L+1}\left[r^{(oi)} + \frac{t^{(oi)}S^c t^{(io)}}{1 - r^{(io)}S^c}\right],$$
(16)

which may be expanded as

$$S_L = (-1)^{L+1}\left[r^{(oi)} + t^{(oi)}S^c t^{(io)}\left(1 + r^{(io)}S^c + \left(r^{(io)}S^c\right)^2 + \ldots\right)\right].$$
(17)

Equation (17) provides a clear physical understanding of the scattering process. It is made up of multiple pathways: reflection off the pure long-range potential; transmission inwards past the long-range potential, followed by a single interaction with the short-range and retransmission out past the long-range potential; then a further series of terms which involve repeated reflections off the long-range potential back towards short range. This last group is responsible for shape resonances when $r^{(io)}S^c$ is close to 1 and successive terms of the sum add constructively. The resonances are damped if $|S^c| < 1$ ($y > 0$). In the limit $S^c \to 0$ the only elastic scattering is reflection off the long-range potential, since all flux transmitted past the long-range potential is lost and not reflected back out.

The total elastic and loss cross-sections may both be expressed in terms of the elastic S-matrix elements,

$$\sigma_{el} = \frac{g\pi}{k^2}\sum_L (2L+1)\,|1 - S_L|^2,$$
(18)

$$\sigma_{loss} = \frac{g\pi}{k^2}\sum_L (2L+1)\left(1 - |S_L|^2\right).$$
(19)

For distinguishable particles, the symmetry factor g is 1 and the sum runs over all values of $L \geqslant 0$; for identical bosons or fermions, g is 2 and the sum runs over only even or only odd values of L, respectively.

3. Results of the single-channel model

Figures 1–3 show the elastic and loss cross-sections for selected values of the loss parameter y, as a function of the short-range phase shift δ^s and the reduced energy $E/\bar{E}$, for distinguishable particles, identical bosons, and identical fermions, respectively. Figures 4–6 show animations of the same quantities, with frames at every value of y from 0 (fully elastic) to 1 (the universal loss regime) in steps of 0.01. The energy scale $\bar{E} = \hbar^2/(2\mu\bar{a}^2)$ is strongly mass-dependent: for example, $\bar{E}/k_B = 61$ mK for He*+Ar [14] but only 97 μK for KRb+KRb [7].

---

[3] The quantity a was termed a background scattering length in [6], but in the presence of closed channels it may nevertheless contain contributions from Feshbach resonances.

Figure 1. Contour plots of the elastic (left) and loss (right) cross-sections for distinguishable particles as a function of reduced energy $E/\bar{E}$ and short-range phase shift δ^s for selected values of the loss parameter y.
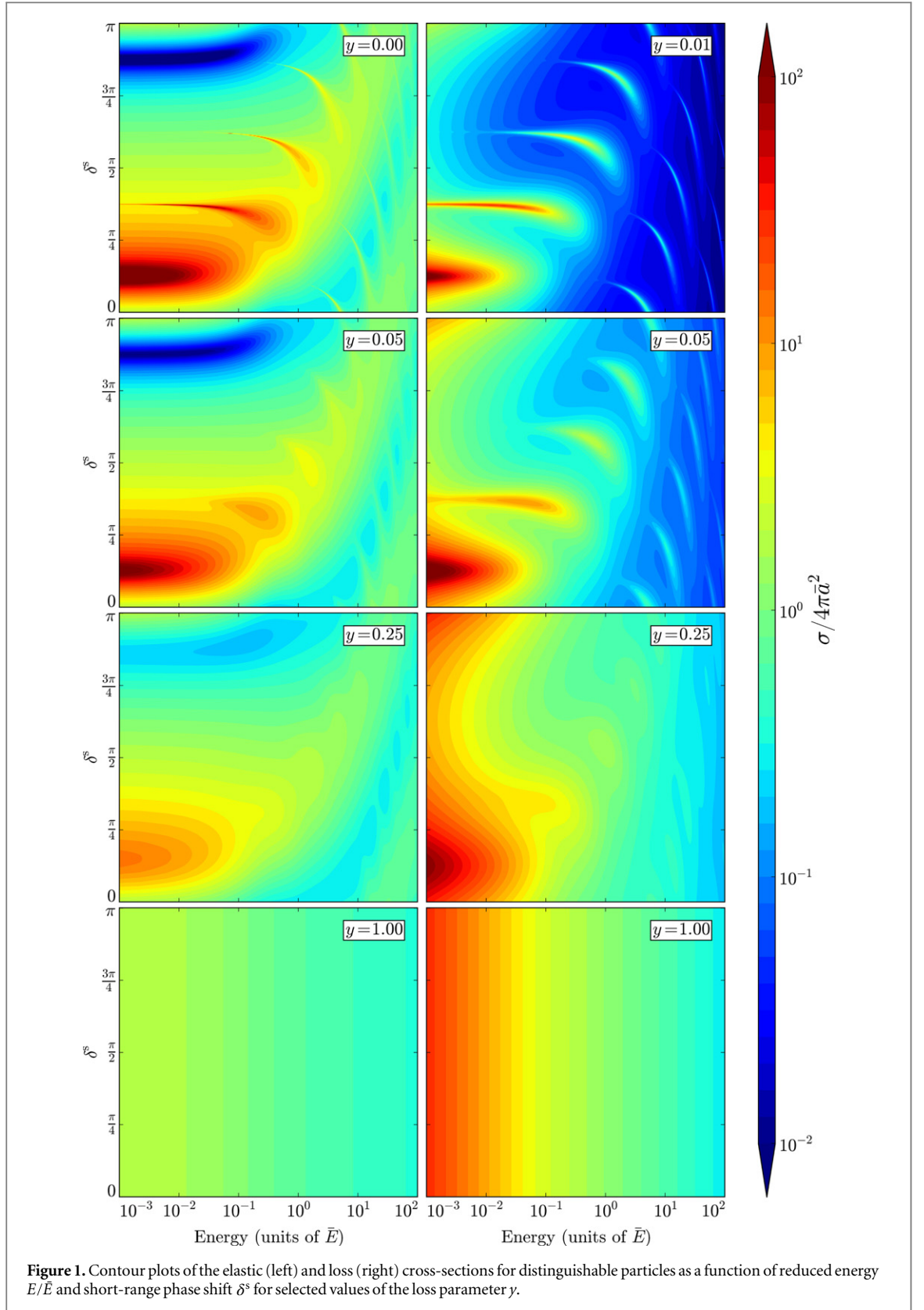
We consider first the case of distinguishable particles. At $y = 0$ (figure 1(a)), low-energy scattering is dominated by s-wave features. There is a large peak near $\delta^s = \pi/8$, which corresponds to infinite scattering length, and a deep trough around $\delta^s = 7\pi/8$, which corresponds to zero scattering length. There is a set of sharp shape resonances that curve towards their zero-energy positions: p-wave at $\delta^s = 3\pi/8$, d-wave at $\delta^s = 5\pi/8$, and further partial waves at increments of $\pi/4$. Thus a shape resonance in partial wave $L + 4$ has the same zero-energy position as that in partial wave L [21], e.g. an h-wave ($L = 5$) shape resonance curves towards the same zero-energy position as the p-wave ($L = 1$) resonance. The plots are cyclic in δ^s with period π, so that the

Figure 2. Contour plots of the elastic (left) and loss (right) cross-sections for identical bosons as a function of reduced energy $E/\bar{E}$ and short-range phase shift δ^{s} for selected values of the loss parameter y.
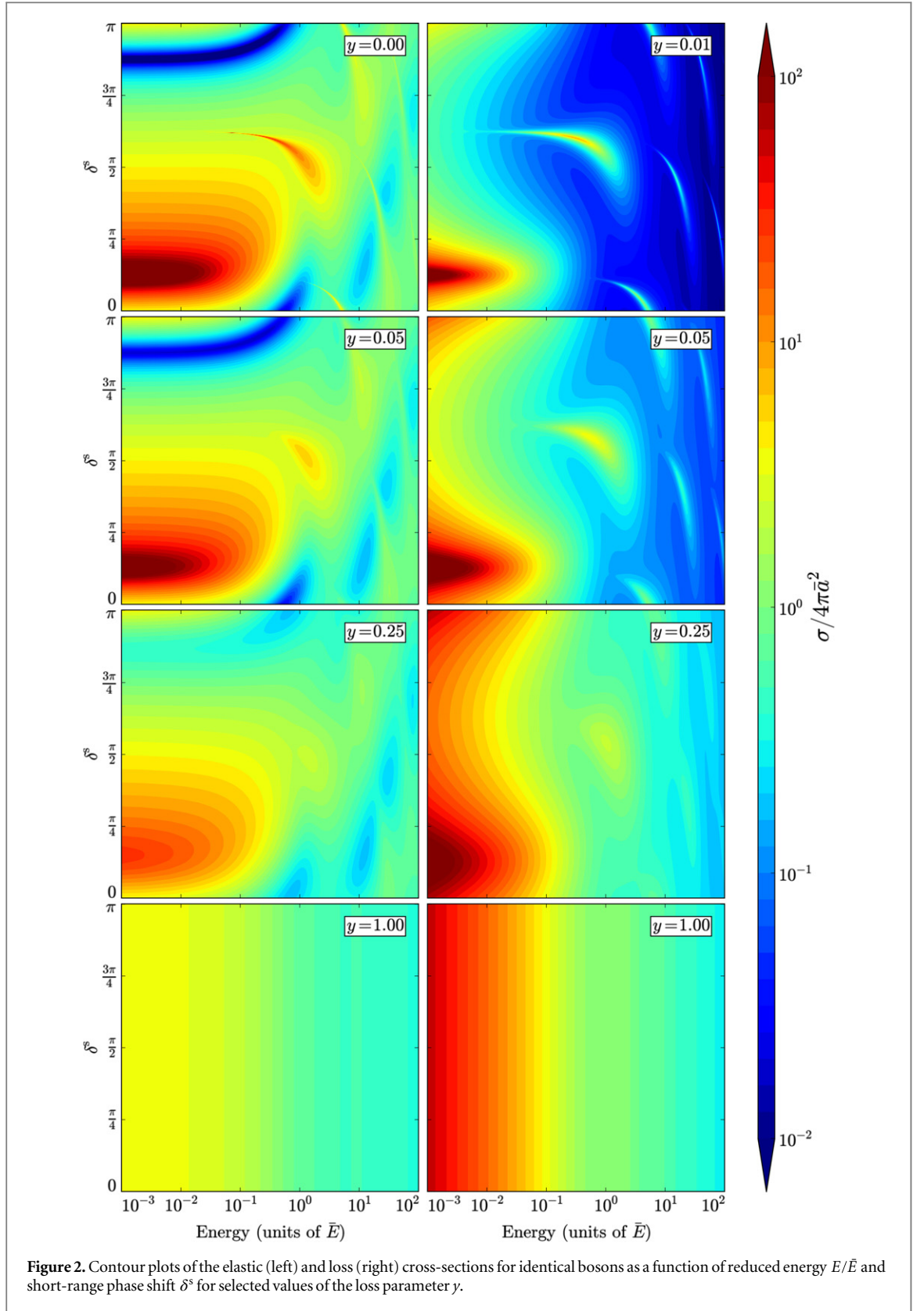
contours along the top edge of each plot are the same as those along the bottom edge. It may be noted that the trough corresponding to zero scattering length curves upwards as a function of energy; this arises because of a Ramsauer–Townsend minimum [22] that occurs in the s-wave cross-section for small negative values of the scattering length.

There is by definition no loss cross-section for $y = 0$; for $y = 0.01$ (figure 1(b)) there is very little loss except close to the shape resonances: little flux is lost in each interaction with the short-range region, so it is only at a shape resonance that there are many interactions with the short-range region and loss becomes important. Shape resonances cause visible features at least as high as $L = 11$ in the plots for $y = 0$ and 0.01. Note that there is a

Figure 3. Contour plots of the elastic (left) and loss (right) cross-sections for identical fermions as a function of reduced energy $E/\bar{E}$ and short-range phase shift δ^s for selected values of the loss parameter y.
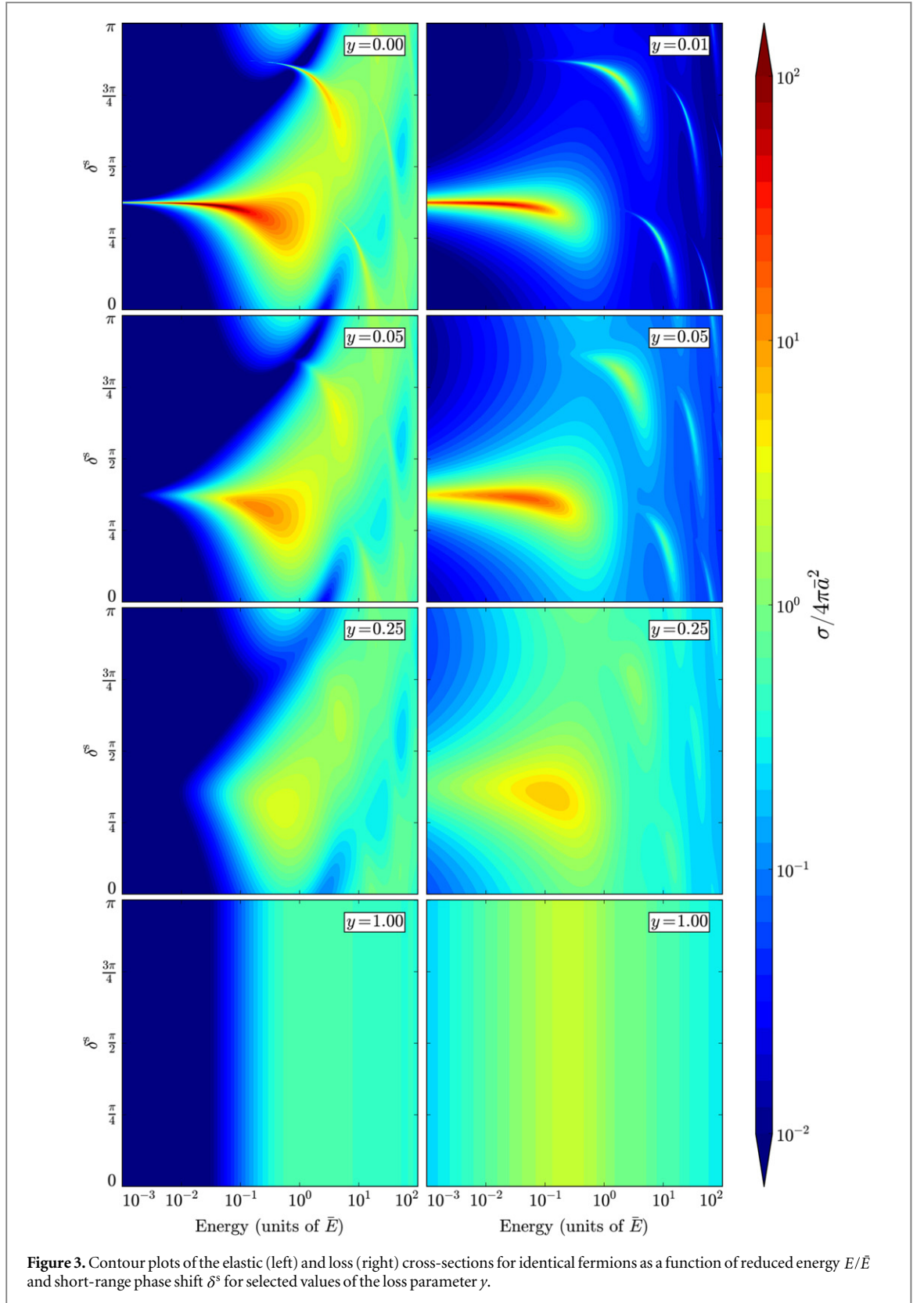
large peak in the s-wave loss near $\delta^s = \pi/8$, even though s-wave collisions cannot have shape resonances *per se*: at low enough energies the long-range potential reflects outgoing flux even with no barrier, so that the multiple interactions with the short-range region that are characteristic of shape resonances can still occur.

As the loss parameter y increases from 0, the features in the cross-sections broaden out and eventually disappear, reaching the 'universal loss' regime described by Idziaszek and Julienne [6]. Most of the features described above are still visible at $y = 0.05$, though the shape resonances are lower and do not persist to such low energy. However, the features have largely washed out by $y = 0.25$. The amplitude of variations in σ_{loss} as a function of δ^s decreases steadily as y increases. It should be noted that, even though $y = 1$ corresponds to

Figure 4. Animations of contour plots of the elastic (left) and loss (right) cross-sections for distinguishable particles as a function of reduced energy $E/\bar{E}$ and short-range phase shift δ^s as the loss parameter y varies from 0 to 1 (available in .mov and .pdf formats at stacks.iop.org/njp/17/045019/mmedia).
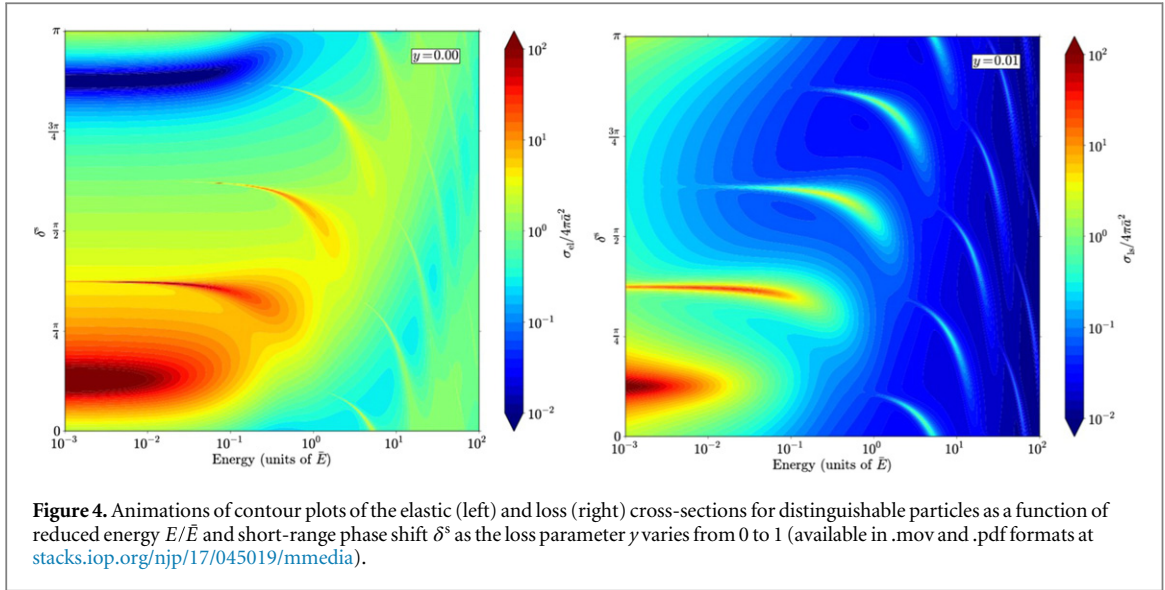
complete loss at short range, it does *not* give the maximum possible overall loss rate. Values of $y < 1$ can sometimes give even faster loss rates because of the possibility of resonant enhancement.

The results for identical bosons (figures 2 and 5) show similar features to those for distinguishable particles, except that there are no odd-L shape resonances. However, the results for identical fermions (figures 3 and 6) are visually very different, because of the lack of an s-wave background at low energy. The shape resonances (this time for odd L only) are therefore even more prominent.

Many experiments use thermal samples. Figure 7 shows the rate constants for loss processes as a function of temperature, for selected values of y, for distinguishable particles (left) and identical fermions (right). The major features of the plots remain, but it may be seen that some of the higher-energy structure is washed out by averaging over kinetic energy. In particular, shape resonances due to partial waves with $L > 3$ are barely visible.
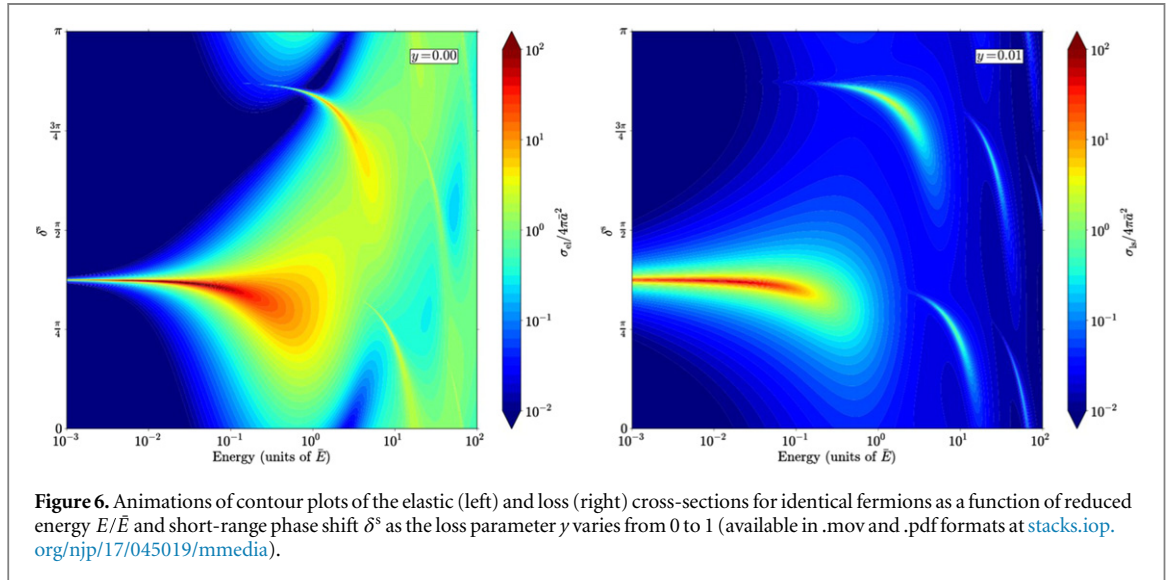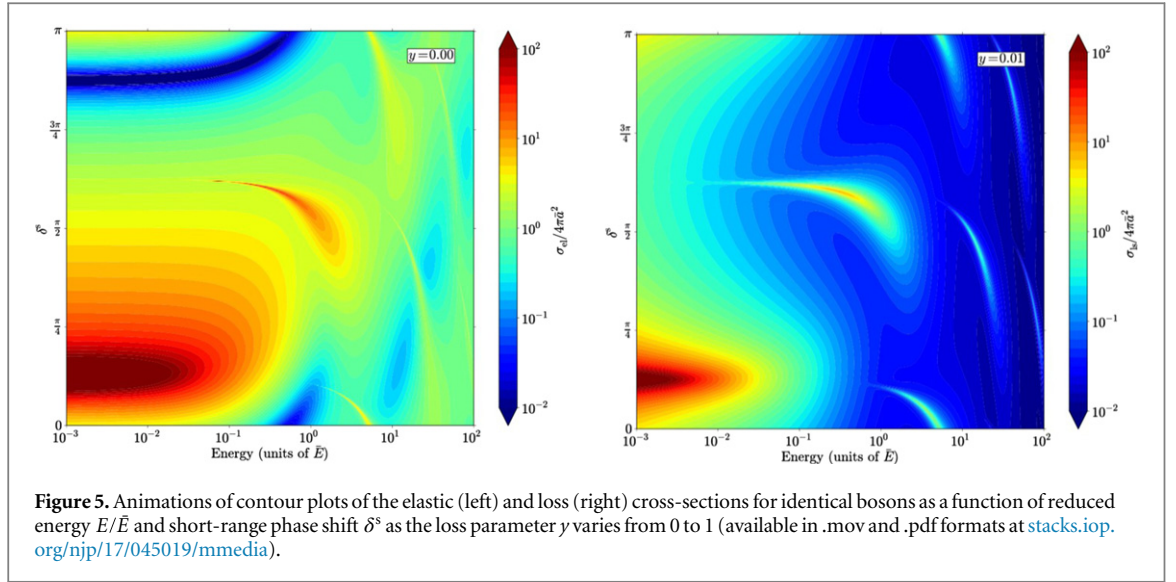
4. Comparison with coupled-channel calculations

Most of the real collision systems of interest in ultracold physics are multichannel in nature and have both shape and Feshbach resonances. It is interesting to consider how far the single-channel model described here can reproduce the results of full coupled-channel calculations in such systems. To explore this, we have carried out full coupled-channel calculations on field-free rotationally inelastic collisions in the system Li+LiH. This is a strongly coupled system with a highly anisotropic potential energy surface [23]. In previous work, we calculated elastic and inelastic collision cross-sections of ^{7}LiH+^{7}Li with the molecules initially in the ground state and the first rotationally excited state [24]. In the present work, we extend these calculations to consider LiH molecules initially in higher rotational states j, so that there are many inelastic (loss) channels available. The calculations are carried out with the MOLSCAT package [25], using the same methods and basis sets for solving the coupled-channels as described in [24]. Cross-sections are calculated by summing contributions from partial waves labelled by the total angular momentum J; the sum converges by $J = 13$ at collision energies up to 1 K for the initial rotational states considered here. We use the potential energy surface from [23], except that we introduce a scaling factor λ that allows us to sample different possible values of the short-range phase shift δ^s[4].

Figure 8 shows the calculated elastic and total inelastic cross-sections for Li+LiH collisions for initial rotational levels $j = 0$, 3 and 6 at kinetic energies $E/k_B = 1$ mK and 50 mK as the scaling factor λ is varied across the range $0.95 < \lambda < 1.05$. The length and energy scales for Li+LiH are $\bar{a} = 16.2$ Å and $\bar{E}/k_B = 24.5$ mK, giving a p-wave barrier height of 6.1 mK. Rotationally inelastic collisions are dominated by couplings at distances much smaller than $\bar{a}$. $E/k_B = 1$ mK is in the s-wave regime, so the cross-sections for initial $j = 0$ show very large peaks and deep troughs. These correspond to poles and zeroes in the s-wave scattering length as successive atom-diatom bound states pass through threshold and cause Feshbach resonances. At $E/k_B = 50$ mK, peaks and troughs are still visible, but are less pronounced because of contributions from higher partial waves and the overall k^{-2} factor in the expressions for cross-sections [26].

---

[4] In scaling the potential, we keep the long-range part fixed (equation (2) and table IV of [23]), and scale the remainder of the potential by a factor λ. This ensures that the Van der Waals length and energy do not vary.

Figure 5. Animations of contour plots of the elastic (left) and loss (right) cross-sections for identical bosons as a function of reduced energy $E/\bar{E}$ and short-range phase shift δ^s as the loss parameter y varies from 0 to 1 (available in .mov and .pdf formats at stacks.iop.org/njp/17/045019/mmedia).

Figure 6. Animations of contour plots of the elastic (left) and loss (right) cross-sections for identical fermions as a function of reduced energy $E/\bar{E}$ and short-range phase shift δ^s as the loss parameter y varies from 0 to 1 (available in .mov and .pdf formats at stacks.iop.org/njp/17/045019/mmedia).
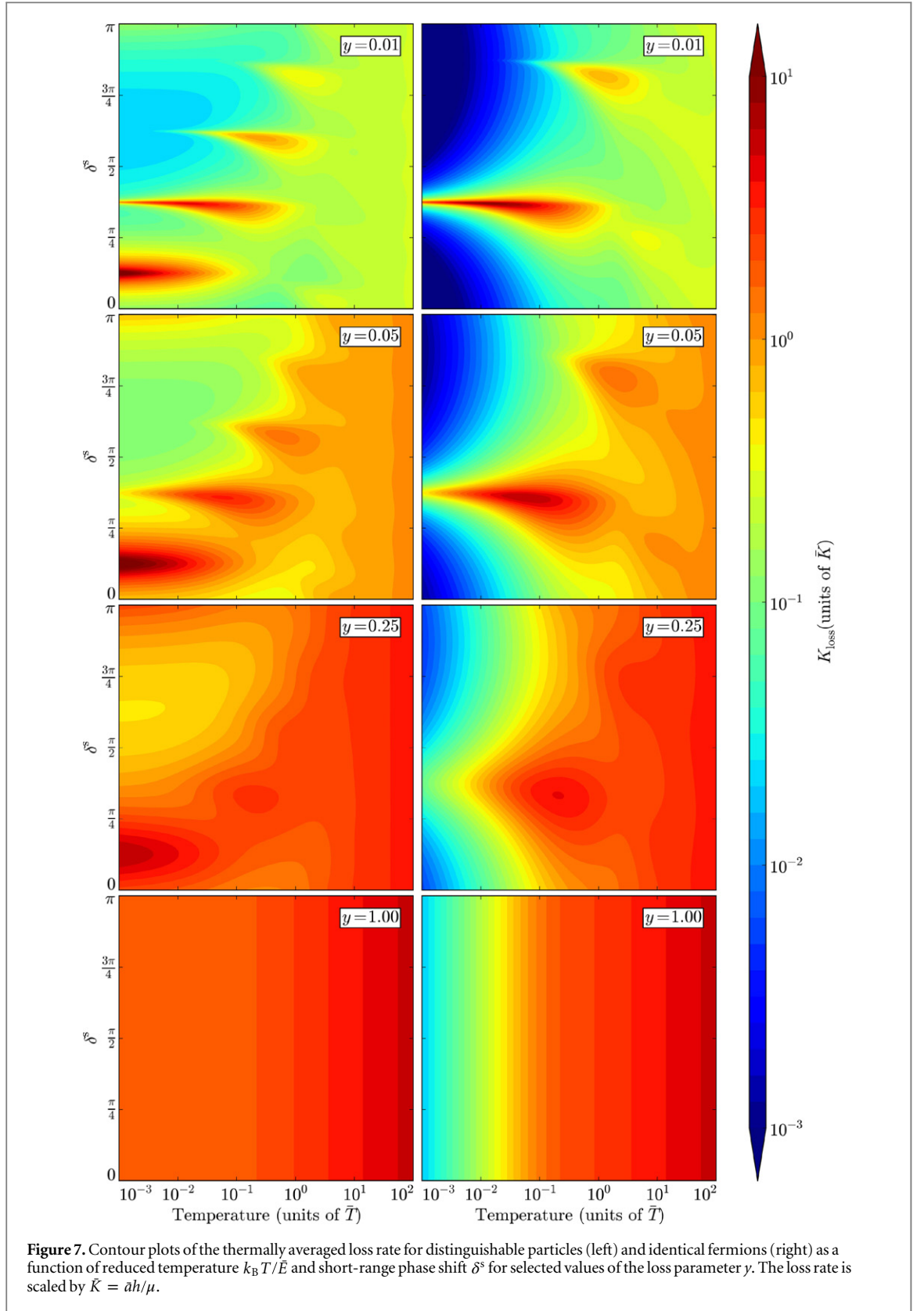
For successively higher initial j values, the number of inelastic channels increases and inelastic scattering becomes progressively stronger. The poles in scattering length that occur for initial $j = 0$ are replaced by finite oscillations that diminish in amplitude as the inelasticity increases [27]. The amplitude of the oscillations in the cross-sections thus decreases as initial j increases, even in the s-wave regime.
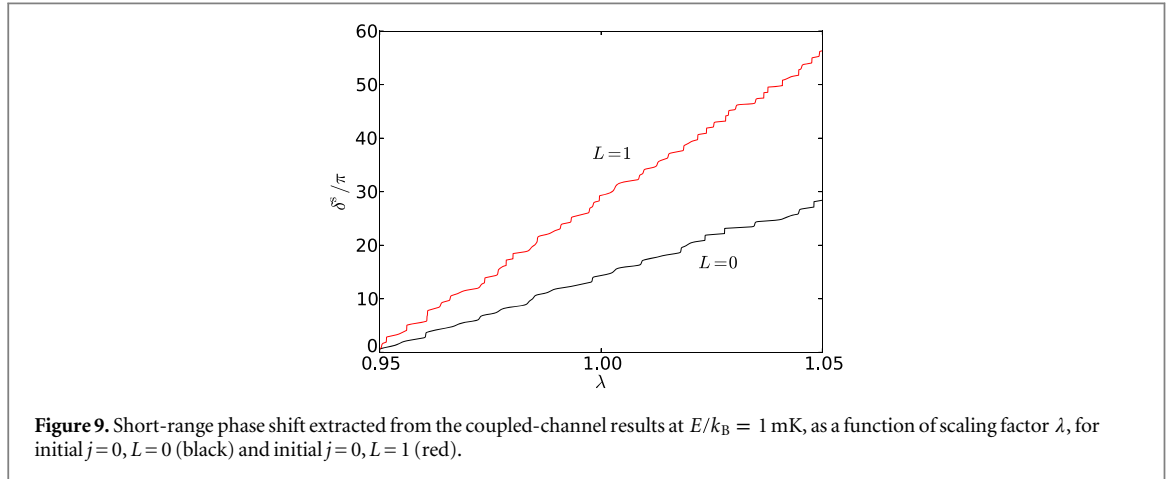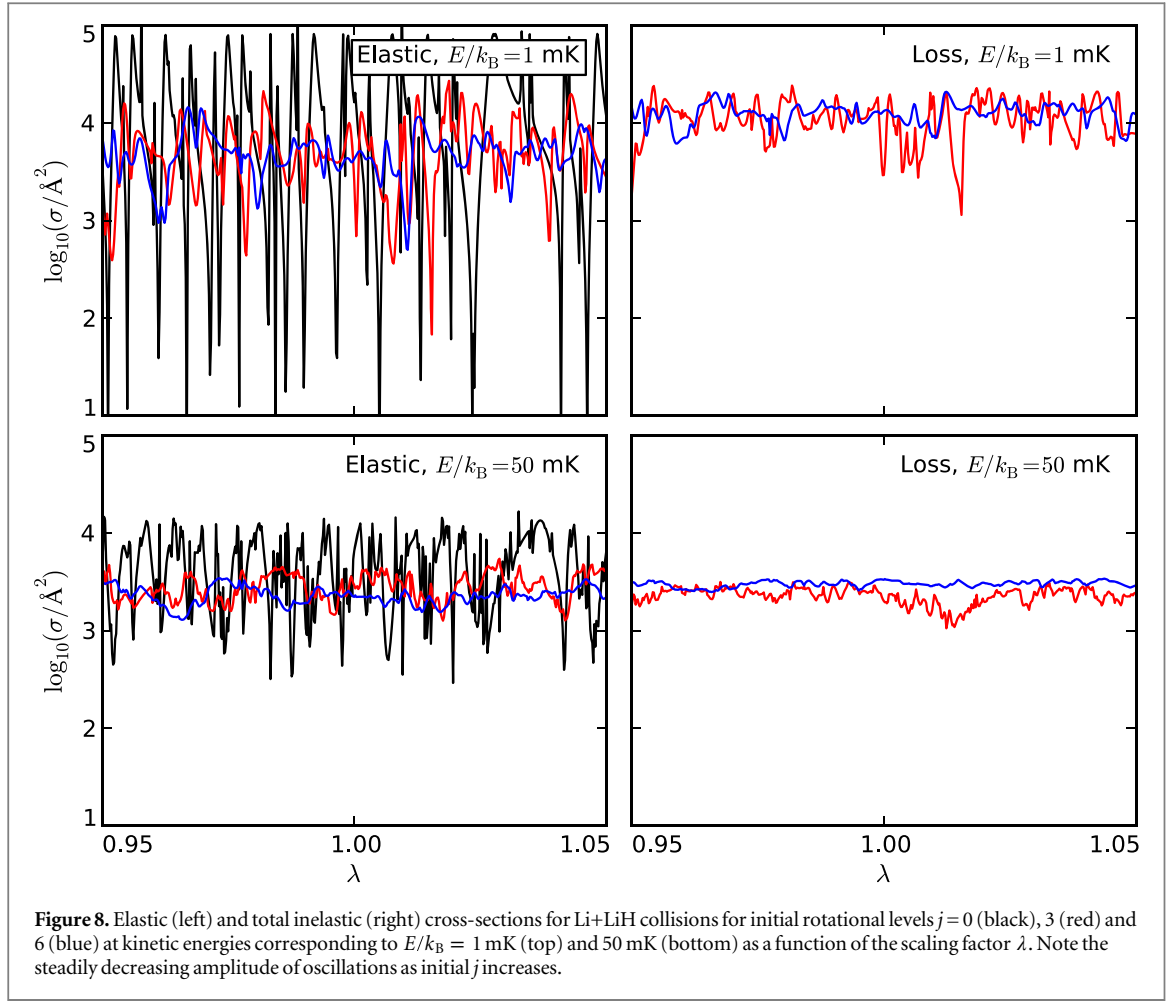
The interaction potential of [23] has an estimated uncertainty of only 0.05%, which is unusually precise for potentials from electronic structure calculations. In cases where the uncertainty is 1 to 5%, which is more typical, it is sufficient to span many oscillations in the cross-sections in a plot such as figure 8. Under these circumstances it is not meaningful to regard the results of scattering calculations on a single potential as predictions for the physical system, and it is essential to understand the *range* of results that may be obtained across the uncertainties in the potential [28, 29]. It is clear from figure 8 that the range of possible results is very large for purely elastic collisions in the s-wave regime, but diminishes both when loss is present (for initial $j > 0$) and when there are significant contributions from several partial waves [26].

It is possible to extract values of the short-range phase shift δ^s and the loss parameter y from coupled-channel results by inverting equation (16) for a particular channel. The lower (black) line in figure 9 shows the short-range phase extracted from the coupled-channel results for initial $j = 0$, $L = 0$ across the range of scaling factors λ considered. Feshbach resonances appear as an increase of π in δ^s over a small range of λ. There are 22 resonances of various widths across the range $0.95 < \lambda < 1.05$, superimposed on a steadily increasing background. The widths of the resonances are comparable to their spacings with respect to both energy and λ scaling, so that even s-wave scattering is influenced by resonance effects for most values of λ. It may be noted that the corresponding resonances in the long-range phase shift have widths that are reduced near threshold [30] and

Figure 7. Contour plots of the thermally averaged loss rate for distinguishable particles (left) and identical fermions (right) as a function of reduced temperature $k_B T/\bar{E}$ and short-range phase shift δ^s for selected values of the loss parameter y. The loss rate is scaled by $\bar{K} = \bar{a}h/\mu$.

are strongly energy-dependent. By contrast, the resonances in the short-range phase shift have widths that are only weakly energy-dependent and correspond to the widths of the features in low-energy cross-sections.

In a multichannel system, the scattering for $L > 0$ is not fully determined by the value of δ^s obtained for $L = 0$. The upper (red) line in figure 9 shows the short-range phase shift obtained by inverting equation (16) for initial $j = 0$, $L = 1$. All the resonances that were present for $L = 0$ appear again, shifted to slightly higher λ and often with somewhat different widths. However, there are 24 additional resonances. The variation of δ^s with L prevents the single-channel model giving accurate energy-dependent cross-sections for a specific interaction

Figure 8. Elastic (left) and total inelastic (right) cross-sections for Li+LiH collisions for initial rotational levels $j = 0$ (black), 3 (red) and 6 (blue) at kinetic energies corresponding to $E/k_B = 1$ mK (top) and 50 mK (bottom) as a function of the scaling factor λ. Note the steadily decreasing amplitude of oscillations as initial j increases.

Figure 9. Short-range phase shift extracted from the coupled-channel results at $E/k_B = 1$ mK, as a function of scaling factor λ, for initial $j = 0$, $L = 0$ (black) and initial $j = 0$, $L = 1$ (red).

potential, even for initial $j = 0$. In addition, for $j > 0$ the value of y obtained by inverting equation (16) is a fast function of λ, even in the s-wave regime, and is also L-dependent. Nevertheless, it is useful to compare the *distribution* of elastic and inelastic cross-sections obtained from coupled-channel calculations (as λ is varied over the range shown in the figures) with that obtained from the single-channel model (as δ^s is varied from 0 to π for a given value of y). Figure 10 shows this comparison for the mean and mean ±1 standard deviation of $\log_{10} \sigma_{el}$ as a function of collision energy for the case of initial $j = 0$, where there are no inelastic channels, so $y = 0$. It may be seen that the single-channel model (with no adjustable parameters whatsoever) quite accurately reproduces the energy-dependence of both the mean and standard deviation, despite the fact that most of the structure in figure 8 comes from Feshbach resonances rather than shape resonances.

Figure 10. Mean values and mean ±1 standard deviation of $\log_{10}(\sigma_{el}/\text{Å}^2)$ from the single-channel model with $y = 0$ (red), compared with the corresponding quantities from coupled-channel calculations for Li+LiH collisions with initial $j = 0$ (black).

Figure 11. Mean values and and mean ± 1 standard deviation of $\log_{10}(\sigma_{el}/\text{Å}^2)$ (left) and $\log_{10}(\sigma_{loss}/\text{Å}^2)$ (right) from the single-channel model (red) for collision energies $E/k_B = 1$ mK (top) and 50 mK (bottom) as a function of y compared with the corresponding quantities from coupled-channel calculations for for Li+LiH collisions with initial $j = 6$ (black horizontal lines). The vertical grey lines indicate $y = 0.54$, which gives the best agreement between the single-channel model and coupled-channel calculations for $j = 6$ at low energy.

For higher initial j, where inelastic scattering is possible, we need to choose a value of y before comparing the coupled-channel and single-channel results. The upper panels of figure 11 show the mean and mean ± 1 standard deviation for log σ_{el} and log σ_{loss} for initial $j = 6$ at $E/k_B = 1$ mK from coupled-channel calculations (horizontal lines), compared with those calculated from the single-channel model as a function of y (converging lines). It may be seen that $y \approx 0.54$ approximately reproduces the low-energy distributions. The lower panels of figure 11 show the corresponding plots at 50 mK; the single-channel model with $y = 0.54$ still reproduces the distribution of σ_{loss} fairly well, and is also qualitatively correct for σ_{el}, though it somewhat overestimates the standard deviation in this case. The full energy-dependence for $y = 0.54$ is shown in the upper panels of figure 12; there are quantitative differences, but the single-channel model is nevertheless remarkably accurate for the distribution of both elastic and inelastic cross-sections over the range of energies shown. For comparison
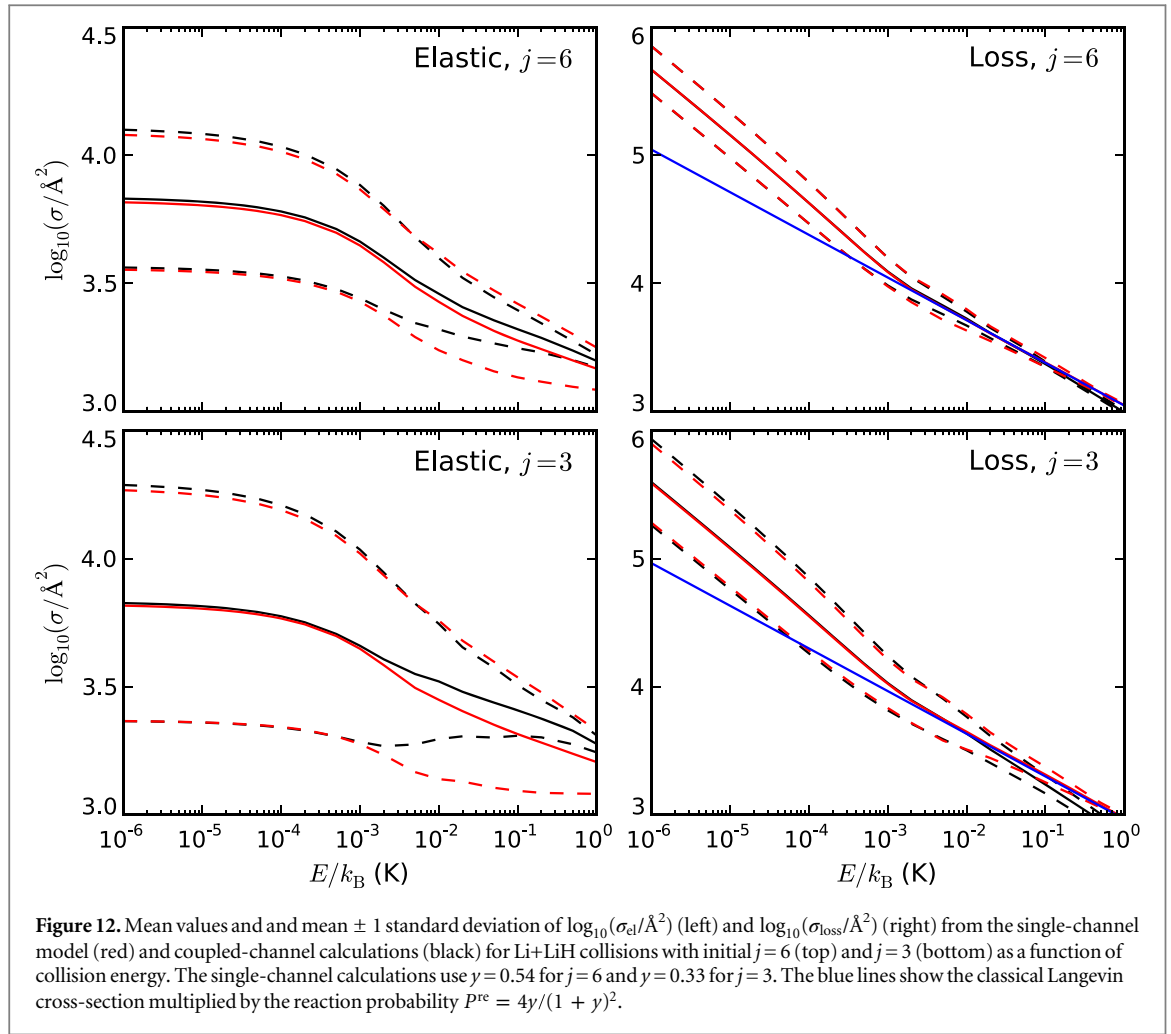
Figure 12. Mean values and and mean ± 1 standard deviation of $\log_{10}(\sigma_{el}/\text{Å}^2)$ (left) and $\log_{10}(\sigma_{loss}/\text{Å}^2)$ (right) from the single-channel model (red) and coupled-channel calculations (black) for Li+LiH collisions with initial $j = 6$ (top) and $j = 3$ (bottom) as a function of collision energy. The single-channel calculations use $y = 0.54$ for $j = 6$ and $y = 0.33$ for $j = 3$. The blue lines show the classical Langevin cross-section multiplied by the reaction probability $P^{re} = 4y/(1 + y)^2$.

figure 12 also shows the classical Langevin cross-section multiplied by the reaction probability $P^{re} = 4y/(1 + y)^2$ [14].

The agreement between the coupled-channel calculations and the single-channel model does deteriorate somewhat for lower values of initial j. This is to be expected, because these cases have fewer open loss channels and it is therefore more likely that flux that is initially lost from the incoming channel will subsequently return to it, violating one of the assumptions of the single-channel model. The lower panels of figure 12 show the case of initial $j = 3$, where the low-energy distribution is reasonably well described by $y = 0.33$. In this case, however, the higher-energy cross-sections calculated from the single-channel model deviate somewhat from the coupled-channel results, particularly for the elastic cross-sections. Nevertheless, qualitative agreement remains.

We have verified that the agreement between the coupled-channel calculations and the single-channel model improves steadily from initial $j = 1$ to 6, as the number of open loss channels increases. Initial $j = 1$ is a special case. In the presence of inelastic scattering, individual Feshbach resonances exhibit both a peak and a dip in the real and imaginary parts of the complex scattering length, and hence in the loss cross-section [27]. When there is a single dominant loss channel, the dip in the s-wave cross-section can be very deep [31] (and reaches $\sigma_{loss} = 0$ when there is only one loss channel). This behaviour skews the distribution of $\log_{10}\sigma_{loss}$ at the low end, particularly for initial $j = 1$. For higher initial j, the effect is reduced by additional loss channels, and at higher energies it is reduced by contributions from higher partial waves.

5. Conclusions

Single-channel models of inelastic and reactive scattering, based on QDT and a single parameter representing short-range loss, provide a powerful approximate approach to understanding complicated collision processes at low kinetic energy. We have investigated how these models behave over the full parameter space of kinetic energy, short-range phase shift (which maps to background scattering length) and short-range loss parameter y. We have presented animated contour plots that help to understand how the sensitivity of cross-sections to the background scattering length decreases both as the loss probability increases and with increasing kinetic energy.

We have also carried out coupled-channel calculations on rotationally inelastic Li+LiH collisions, as a prototype strongly coupled collision system, to test the results of the single-channel model. The low-energy elastic and total inelastic (loss) cross-sections are very sensitive to the short-range potential, and oscillate very fast as a function of a potential scaling factor λ. However, the amplitude of the oscillations decreases as the initial rotational quantum number j increases, corresponding to an increasing number of loss channels (and increasing y). The amplitude also decreases as the collision energy increases. The energy dependence of the *distribution* of cross-sections σ, characterized by the mean and standard deviation of $\log_{10}\sigma$ with respect to variations in the potential, is well reproduced by the single-channel model for larger values of initial j. For small j the single-channel model is less accurate but still qualitatively correct.

The present results elucidate the range of behaviour that can be expected for cold elastic and inelastic (or reactive) collisions in complex systems. They also demonstrate that single-channel models with a single short-range loss parameter can correctly reproduce the qualitative features of full-coupled channel calculations in systems with many open channels, including the dependence on collision energy. The quality of agreement improves as the strength of the short-range loss increases. However, specific systems nevertheless show strong sensitivity to the details of the short-range interaction potential, which disappears only in the limit of complete short-range loss.

The present results suggest a remarkable possibility for inferring the behaviour of cold collisions at higher temperatures from calculations in the s-wave regime. For a system with enough open channels to be well described by a single-channel model, it would be possible to perform coupled-channel calculations for incoming $L = 0$ only and use the results (as a function of a potential scaling factor λ) to determine a short-range loss parameter y. The single-channel approach could then be used to predict the range of possible loss rates at higher energy, without the need to carry out explicit coupled-channel calculations for higher initial L.

Acknowledgments

References

[1] Weiner J, Bagnato V S, Zilio S and Julienne P S 1999 *Rev. Mod. Phys.* **71** 1
[2] Chin C, Grimm R, Tiesinga E and Julienne P S 2010 *Rev. Mod. Phys.* **82** 1225
[3] Ospelkaus S, Ni K-K, Wang D, de Miranda M H G, Neyenhuis B, Quéméner G, Julienne P S, Bohn J L, Jin D S and Ye J 2010 *Science* **327** 853
[4] Henson A B, Gersten S, Shagam Y, Narevicius J and Narevicius E 2012 *Science* **338** 234
[5] van de Meerakker S Y T, Bethlem H L, Vanhaecke N and Meijer G 2012 *Chem. Rev.* **112** 4828
[6] Idziaszek Z and Julienne P S 2010 *Phys. Rev. Lett.* **104** 113202
[7] Kotochigova S 2010 *New J. Phys.* **12** 073041
[8] Gao B 2010 *Phys. Rev. Lett.* **105** 263203
[9] Mies F H 1984 *J. Chem. Phys.* **80** 2514
[10] Julienne P S and Mies F H 1989 *J. Opt. Soc. Am.* B **6** 2257
[11] Gao B 2008 *Phys. Rev.* A **78** 012702
[12] Gao B 2010 *Phys. Rev. Lett.* **104** 213201
[13] Idziaszek Z, Quéméner G, Bohn J L and Julienne P S 2010 *Phys. Rev.* A **82** 020703
[14] Jachymski K, Krych M, Julienne P S and Idziaszek Z 2013 *Phys. Rev. Lett.* **110** 213202
[15] Jachymski K, Krych M, Julienne P S and Idziaszek Z 2014 *Phys. Rev.* A **90** 042705
[16] Gao B 2001 *Phys. Rev.* A **64** 010701
[17] Frye M D and Hutson J M 2014 *Phys. Rev.* A **89** 052705
[18] Gao B 1998 *Phys. Rev.* A **58** 1728
[19] Gao B 2003 *Routines to Calculate the AQDT Parameters for an Attractive $1/r^6$ Potential, Version 2* (Ohio: University of Toledo)
[20] Gribakin G F and Flambaum V V 1993 *Phys. Rev.* A **48** 546
[21] Gao B 2000 *Phys. Rev.* A **62** 050702
[22] Mott N F and Massey H S W 1965 *The Theory of Atomic Collisions* 3rd edn (Oxford: Clarendon)
[23] Skomorowski W, Pawłowski F, Korona T, Moszynski R, Żuchowski P S and Hutson J M 2011 *J. Chem. Phys.* **134** 114109
[24] Tokunaga S, Skomorowski W, Moszynski R, Żuchowski P S, Hutson J M, Hinds E A and Tarbutt M R 2011 *Eur. Phys. J.* D **65** 141
[25] Hutson J M and Green S 1994 *MOLSCAT computer program, version 14* Collaborative Computational Project No 6, UK Engineering and Physical Sciences Research Council
[26] Wallis A O G, Longdon E J J, Żuchowski P S and Hutson J M 2011 *Eur. Phys. J.* D **65** 151
[27] Hutson J M 2007 *New J. Phys.* **9** 152
[28] Hutson J M and Soldán P 2007 *Int. Rev. Phys. Chem.* **26** 1
[29] Wallis A O G and Hutson J M 2009 *Phys. Rev. Lett.* **103** 183201
[30] Timmermans E, Tommasini P, Hussein M and Kerman A 1999 *Phys. Rep.* **315** 199
[31] Hutson J M, Beyene M and González-Martínez M L 2009 *Phys. Rev. Lett.* **103** 163201